Supplementary Information (SI) for Inorganic Chemistry Frontiers.

Supplementary Information for

Universal synthesis of coral-like Ternary MOF-Derived Sulfides as efficient OER electrocatalysts

Tianpeng Liu[a], Yangping Zhang[a], Jun Yu[a], Mengyun Hu[a], Zhengying Wu*[b], Xiao Wei[a], Shudi Yu[a], Yukou Du*[a]

[a] College of Chemistry, Chemical Engineering and Materials Science, Soochow University, Industrial Park, Renai Road, Suzhou 215123, P.R. China

[b] Jiangsu Key Laboratory for Environment Functional Materials, School of Materials Science and Engineering, Suzhou University of Science and Technology, Suzhou 215009, China

E-mail: duyk@suda.edu.cn (Y. Du), zywu@mail.usts.edu.cn (Z. Wu).

Experimental

Synthesis of ternary MOF templates.

The synthesis method of the ternary MOF templates is based on adjustments of previous reported research [1]. The $Zn(NO_3)_2$ $6H_2O$ (0.324 mmol), $Ni(NO_3)_2$ $6H_2O$ (0.648 mmol) and $Fe(NO_3)_3$ $9H_2O$(0.324 mmol) are dissolved in 8 mL of N,N-Dimethylformamide (DMF) through sonication labeled as A. Similarly, the powder of 1,3,5-trimesic acid (H_3BTC) is dissolved in 8 mL of DMF labeled as B. The solution A and B are mixed and sonicated for 30 minutes at room temperature, then the mixed solution is heated at 170 °C for 24 h in hydrothermal autoclave reactor. The product is purified through ethanol wishing, centrifugation for three times, finally dried overnight at 60 °C, denoted as FeNiZn. The synthesis method of FeNiCo and FeNiCd exhibited similarities to that of FeNiZn, with the sole distinction being the substitution of $Zn(NO_3)_2$ $6H_2O$ in the reactants with $Co(NO_3)_2$ $6H_2O$ and $Cd(NO_3)_2$ $4H_2O$ respectively.

Synthesis of FeNiZnS trimetallic sulfide.

In a typical MOF-derived sulfide synthesis procedure, the powers of FeNiZn (50 mg) template and C_2H_5NS (50 mg) are dissolved in 15 mL of ethanol. Subsequently, the mixed solution is heated at 150 °C in hydrothermal autoclave reactor and reacted 1, 2 and 3 h, respectively. The products are purified through ethanol wishing, centrifugation for three times, finally dried overnight at 60 °C, designated as FeNiZnS-1, FeNiZnS-2 and FeNiZnS-3 respectively.

Materials and chemicals

Nickel (II) nitrate hexahydrate ($Ni(NO_3)_2$ $6H_2O$, A.R.), Cobalt (II) nitrate hexahydrate ($Co(NO_3)_2$ $6H_2O$, A.R.), Iron (III) nitrate hexahydrate ($Fe(NO_3)_3$ $9H_2O$, A.R.), Zinc (II) nitrate hexahydrate ($Zn(NO_3)_2$ $6H_2O$, A.R.), and Cadmium (II) nitrate tetrahydrate ($Cd(NO_3)_2$ $4H_2O$, A.R.) are purchased from Sigma−Aldrich. Nafion (5% wt) and thioacetamide (C_2H_5NS, A.R.) are obtained from Sinopharm Chemicals Reagent Co, Ltd, China. Potassium hydroxide (KOH, G.R.), *N, N*-Dimethylformamide (DMF,

99.5%), 1,3,5-trimesic acid (H_3BTC, 99%), and ethanol (A.R.) are purchased from Alfa Aesar.

Physical Characterizations

The microscopic morphology of the samples is obtained by Transmission electron microscope (TEM, HT-7700) and High-resolution Transmission electron microscope (HRTEM, Talos F200X G2). The elemental composition and phases of the electrocatalysts are obtained by scanning electron microscope (SEM, Regulus 8230) and X-ray diffraction (XRD, X Pert-Pro MPD). The surface elemental valence states of the samples are determined by X-ray photoelectron spectroscopy (XPS, EXCALAB 250 XI).

Electrochemical measurements

All electrochemical experiments are collected by the electrochemical workstation (CHI 760E Chenhua, Shanghai) in 1 mol/L KOH alkaline solution at room temperature. The electrodes in the electrochemical tests are working electrode (glassy carbon electrode, diameter: 5 mm, area: 0.196 cm^2), counter electrode (carbon rod), and reference electrode (Ag/AgCl), respectively. To prepare the catalyst ink, 3 mg of catalyst and 3 mg carbon black are dispersed in 1 mL of a solution containing 0.99 mL of ethanol and 10 μL of Nafion, followed by ultrasonication for 0.5 h (All catalyst inks are prepared according to this method). Subsequently, 10 μL of catalytic ink is dropped on the glassy carbon electrode and dried at room temperature.

All potentials are converted to the reversible hydrogen electrode (RHE) using the following formula: E (RHE) = E (Ag/AgCl) + 0.197 + 0.059 × pH. The linear sweep voltammetry curves (LSV) are measured at a scan rate of 5 mV s^{-1} and corrected with 95% iR compensation. Moreover, the double layer capacitance (C_{dl}) value is obtained from cyclic voltammograms (CVs) under scan rates (10 - 50 mV s^{-1}) and specific capacitance (C_s) is chosen based on previously reported work. The electrochemically active surface area (ECSA) is calculated by the equation: ECSA=C_{dl} / C_s [2]. The Shirley background is subtracted from the measured spectra. The position of the center of the valence band is given by $\varepsilon_d = \int_{-\infty}^{\infty} n_d(\varepsilon)\varepsilon\, d\varepsilon / \int_{-\infty}^{\infty} n_d(\varepsilon) d\varepsilon$, where $n_d(\varepsilon)$ is the XPS-

intensity after background subtraction [3]. The chronopotentiometry (CP) test measured the potential at a current density of 10 mA cm^{-2} to assess the electrochemical stability of the catalysts.

Supporting Figure and Tables

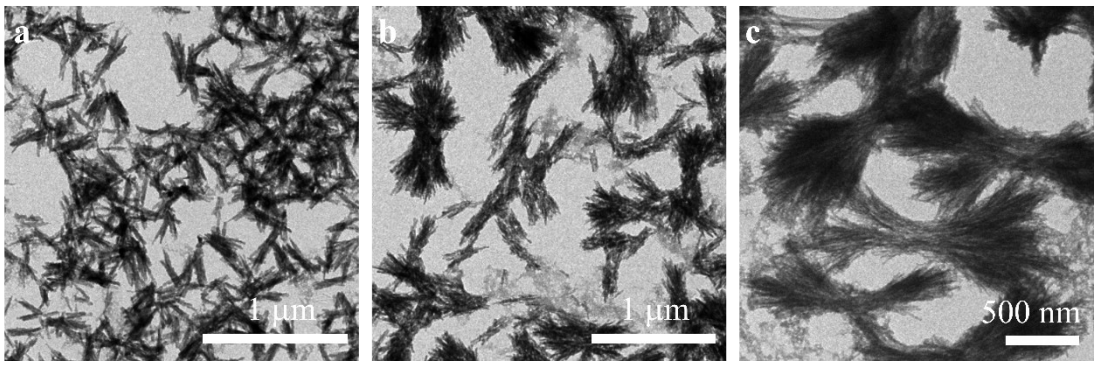

Figure. S1 TEM images of trimetallic template (a) FeNiZn, (b) FeNiCo (c) FeNiCd.

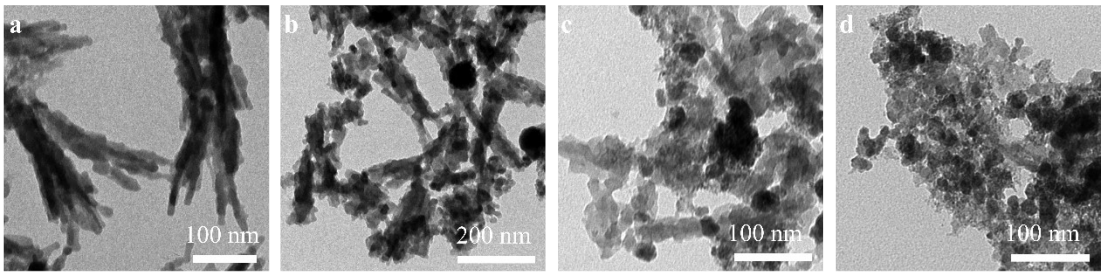

Figure. S2 TEM images of trimetallic sulfide with different reaction time, (a) FeNiZn, (b) FeNiZnS-1 (c) FeNiZnS-2 and (d) FeNiZnS-3.

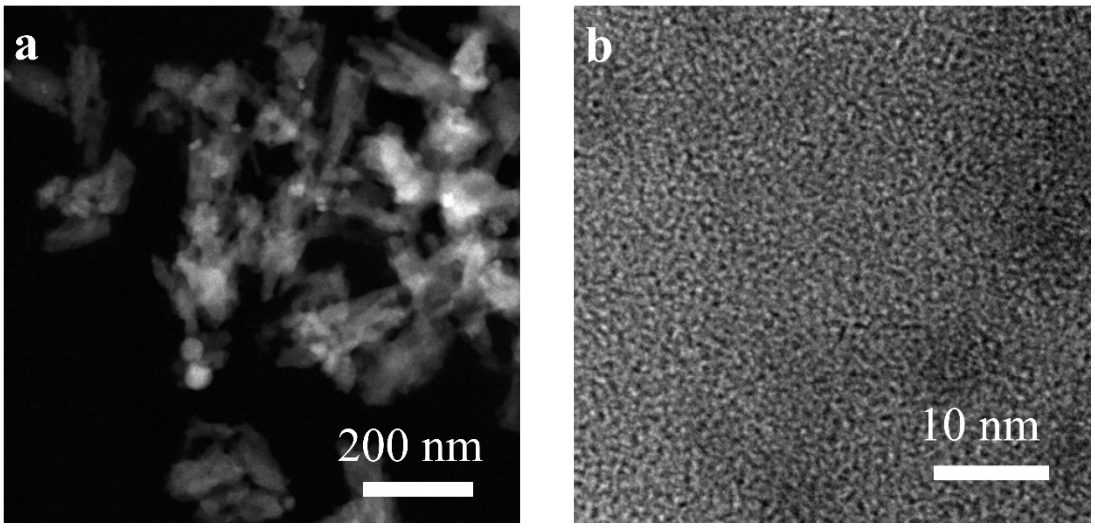

Figure. S3 Physical characterization of FeNiZnS-1. (a) HAADF-STEM, (b) HRTEM.

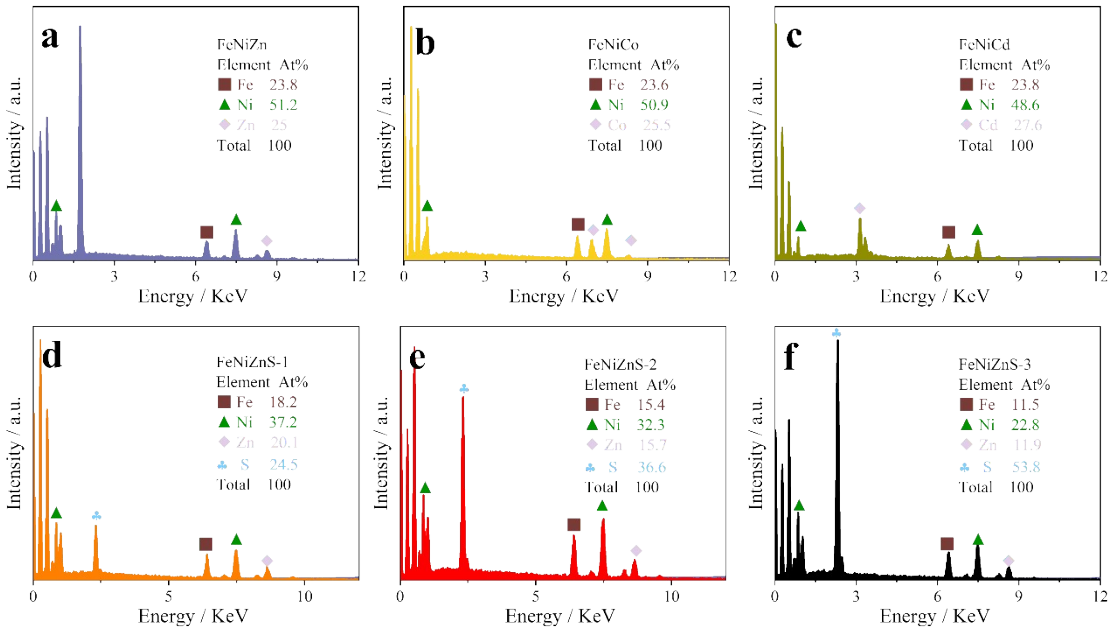

Figure. S4. SEM-EDS spectrum of trimetallic template and sulfides (a) FeNiZn, (b) FeNiCo, (c) FeNiCd, (d) FeNiZnS-1, (e) FeNiZnS-2 and (f) FeNiZnS-3.

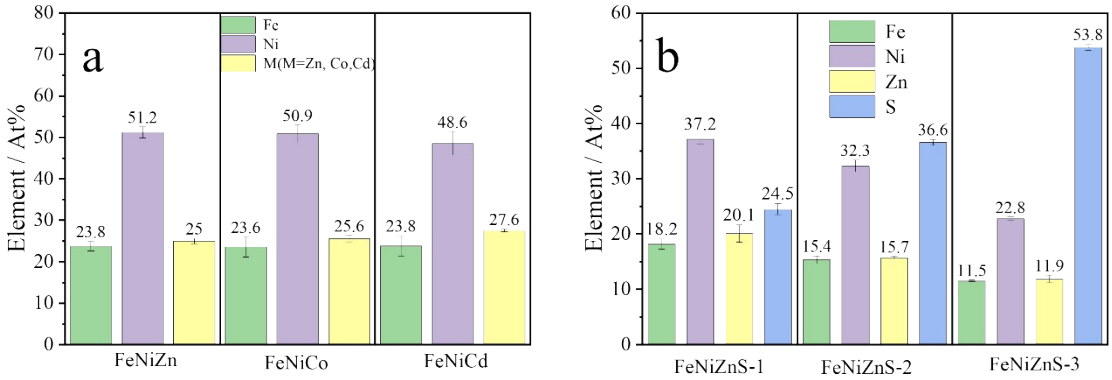

Figure. S5 Error estimates of elements composition.

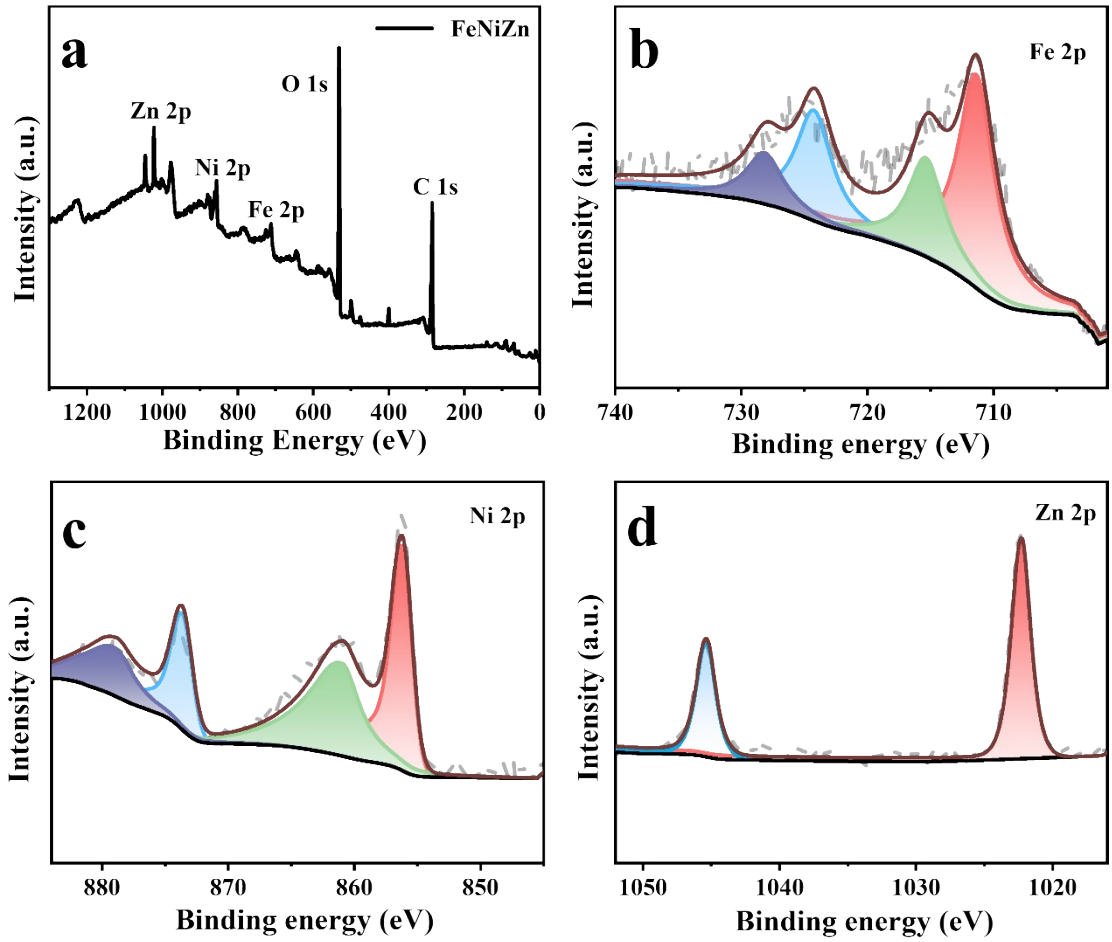

Figure. S6 XPS spectra of FeNiZn (a) survey scan, (b) Fe 2p, (c) Ni 2p and (d) Zn 2p.

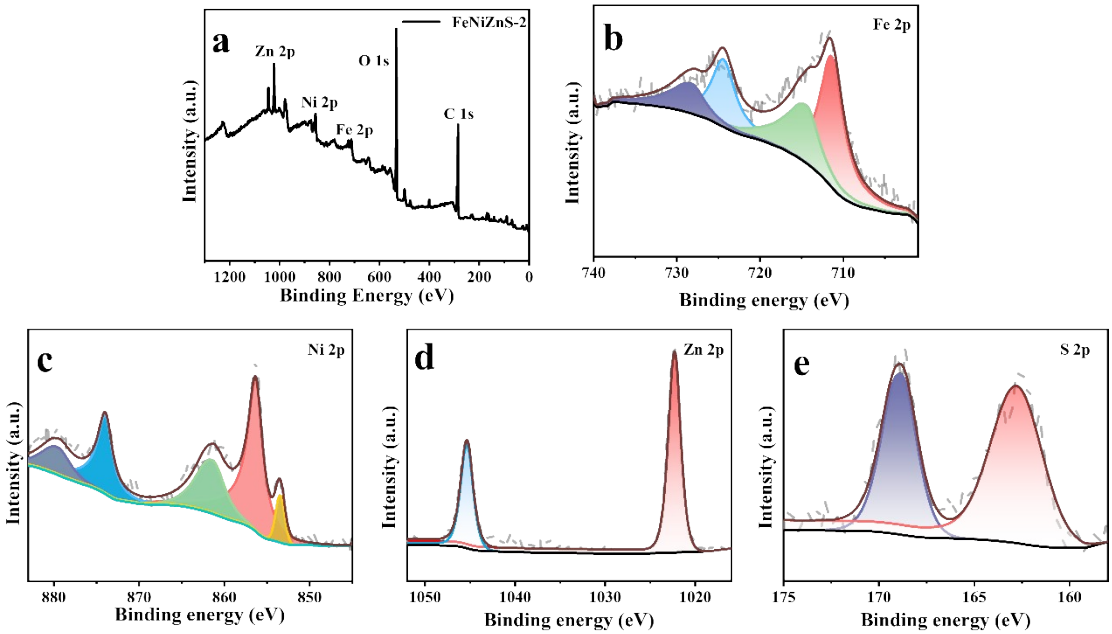

Figure. S7 XPS spectra of FeNiZnS-2 (a) survey scan, (b) Fe 2p, (c) Ni 2p, (d) Zn 2p and (e) S 2p.

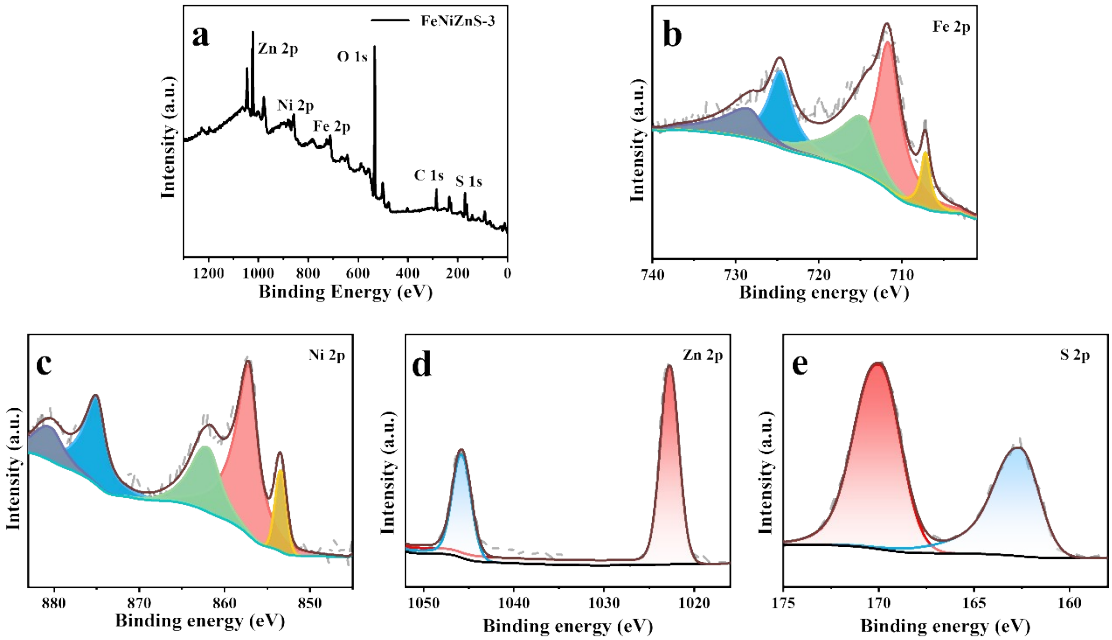

Figure. S8 XPS spectra of FeNiZnS-3 (a) survey scan, (b) Fe 2p, (c) Ni 2p, (d) Zn 2p and (e) S 2p.

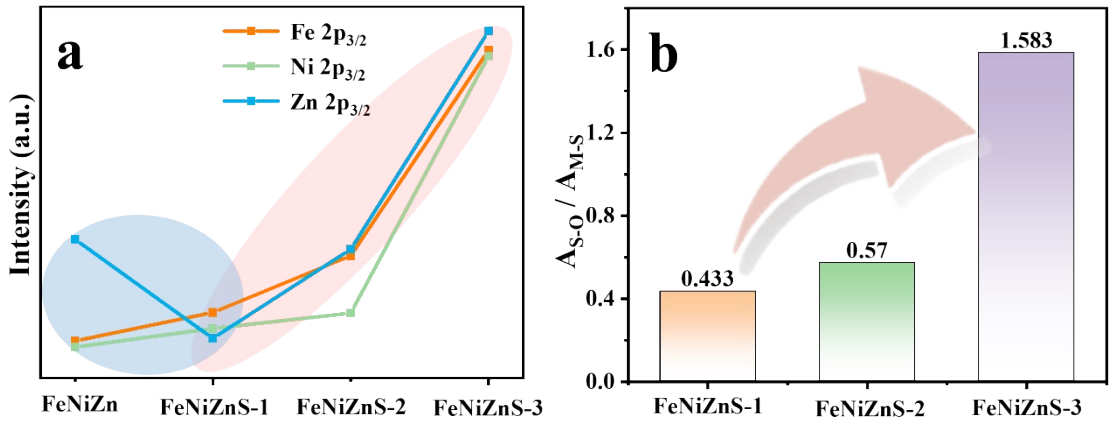

Figure. S9 (a) The change of binding energy of $2p_{3/2}$ in each sample. (b) Ratio of S-O peak to M-O peak area in S 2p level of trimetallic sulfides.

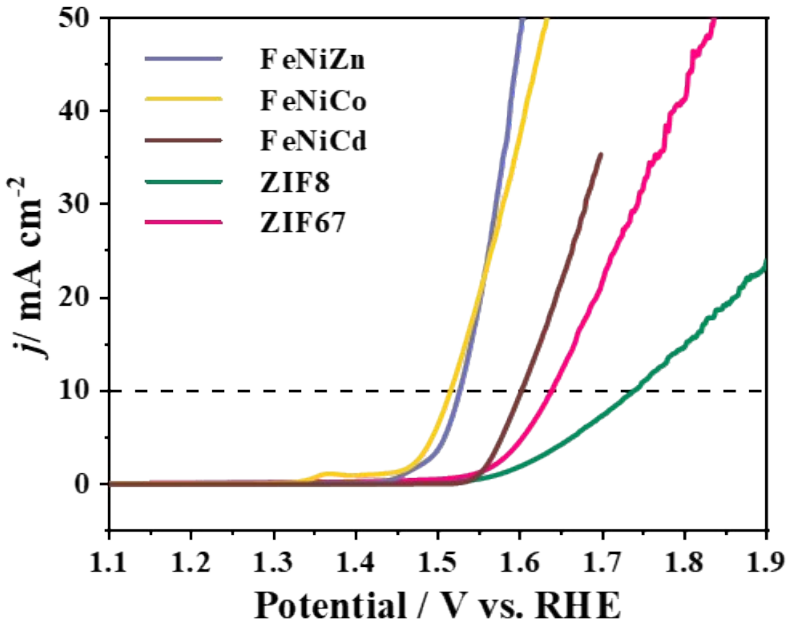

Figure. S10 The OER performance of monometallic and trimetallic MOF template.

Table. S1 The fitting results of samples by fitting with the proposed equivalent circuit.

Catalysts	R_s (Ω)	R_{ct}(Ω)
FeNiZn	6.01	74.37
FeNiCo	7.80	32.47
FeNiCd	9.02	186.2
FeNiZnS-1	6.49	9.14
FeNiZnS-2	5.89	15.12
FeNiZnS-3	5.59	19.37
RuO_2	7.62	120.8

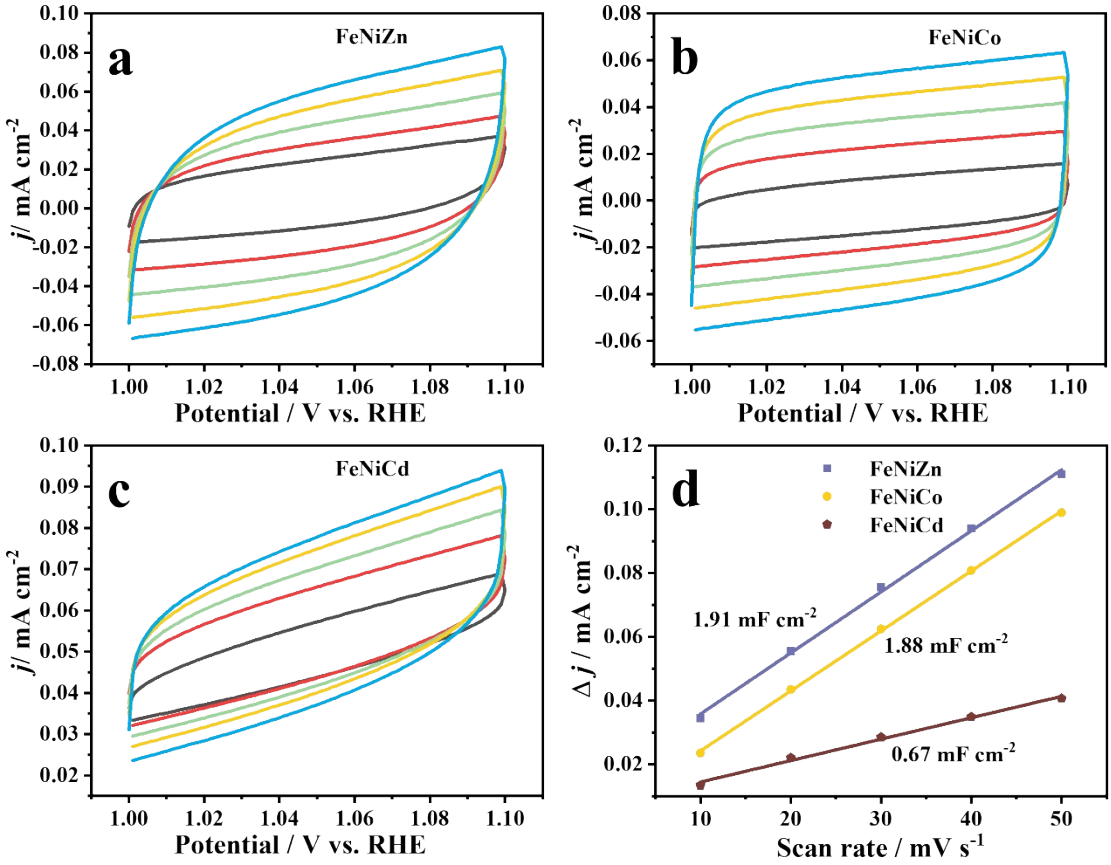

Figure. S11 CV curves of (a) FeNiZn, (b) FeNiCo, (c) FeNiCd in 1 M KOH solution at different scan rates. (d) C_{dl} value of trimetallic MOFs templates.

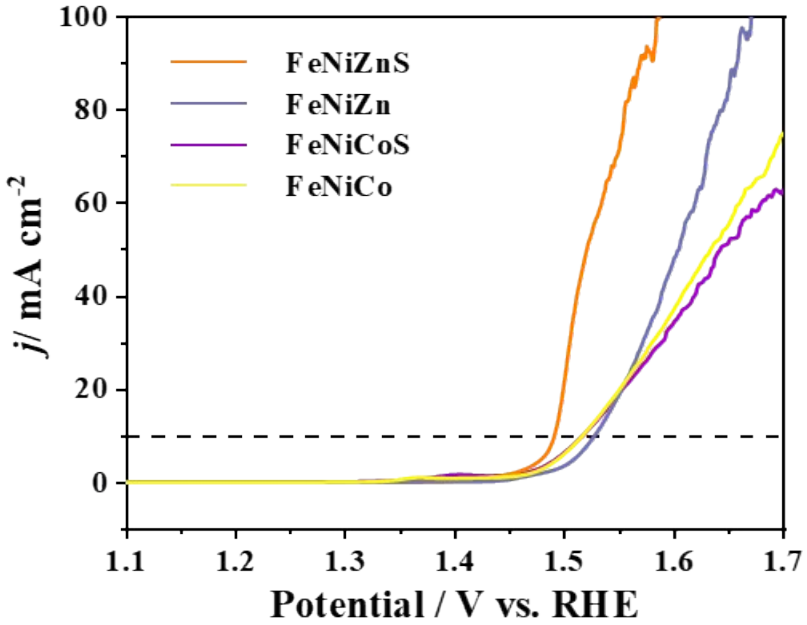

Figure. S12 The OER performance of FeNiZnS and FeNiCoS and trimetallic templates.

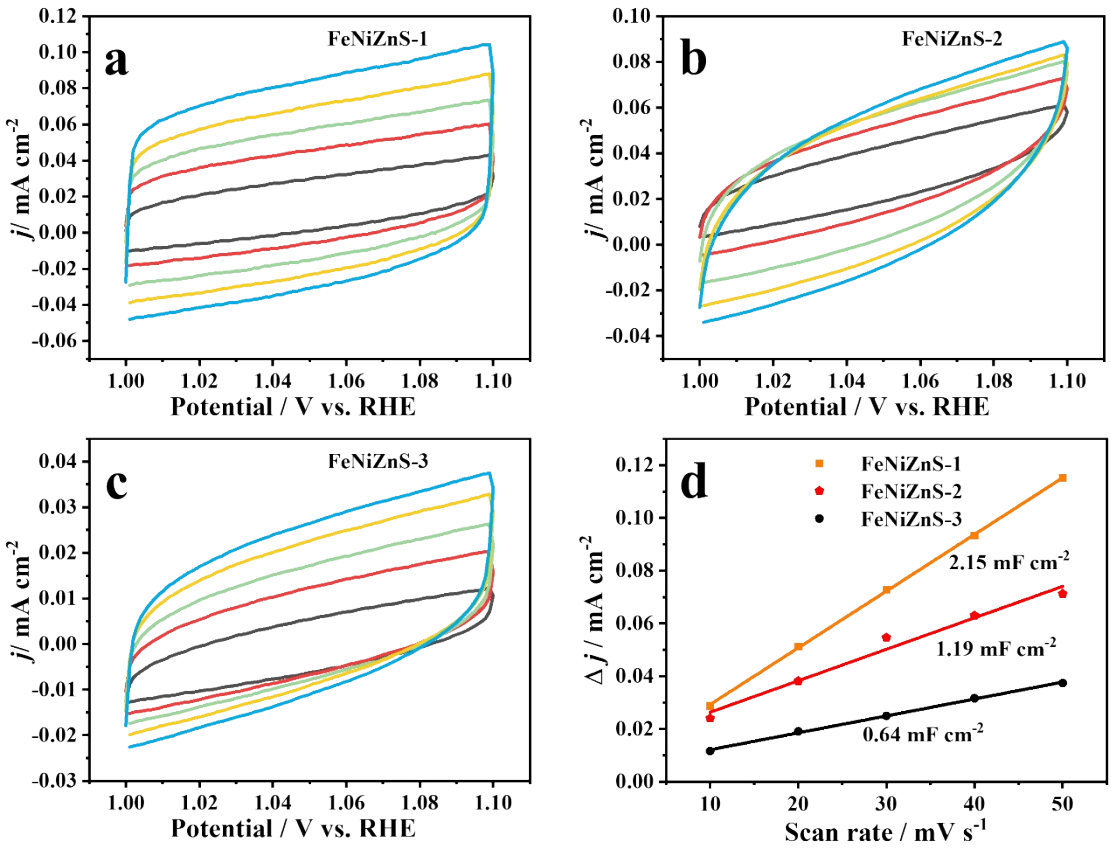

Figure. S13 CV curves of (a) FeNiZnS-1, (b) FeNiZnS-2, (c) FeNiZnS-3 in 1 M KOH solution at different scan rates. (d) C_{dl} value of trimetallic sulfide.

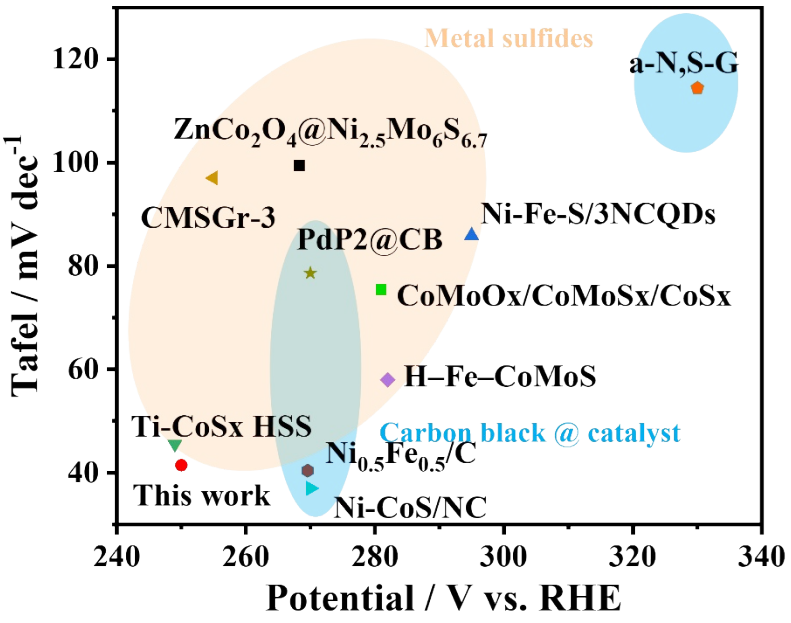

Figure. S14 Electrocatalytic OER activity of this work and previous reported works of sulfides catalysts.

Table. S2 Electrocatalytic OER activity of this work and previous reported works of sulfides catalysts.

Catalysts	η (mV) at 10 mA cm^{-2}	Tafel Slope (mV dec^{-1})	Reference
FeNiZnS-1	249	41.45	This work
$CoMoO_x/CoMoS_x/CoS_x$	281	75.4	[4]
Ni-Fe-S/3NCQDs	295	85.9	[5]
Ti-CoSx HSS	249	45.5	[6]
H–Fe–CoMoS	282	58	[7]
CMSGr-3	255	97	[8]
Ni-CoS/NC	270	37	[9]
$Ni_{0.5}Fe_{0.5}/C$	269.6	40.43	[10]
PdP_2@CB	270	78.6	[11]
a-N, S-G	330	114.4	[12]
$ZnCo_2O_4$@$Ni_{2.5}Mo_6S_{6.7}$	268.3	99.4	[13]

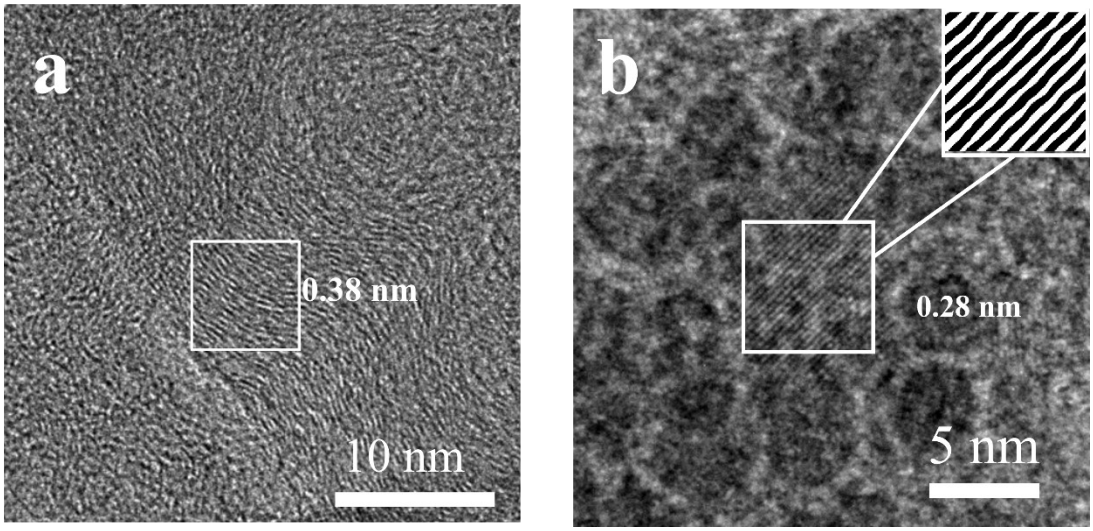

Figure. S15 The HR-TEM images for FeNiZnS-1/AO.

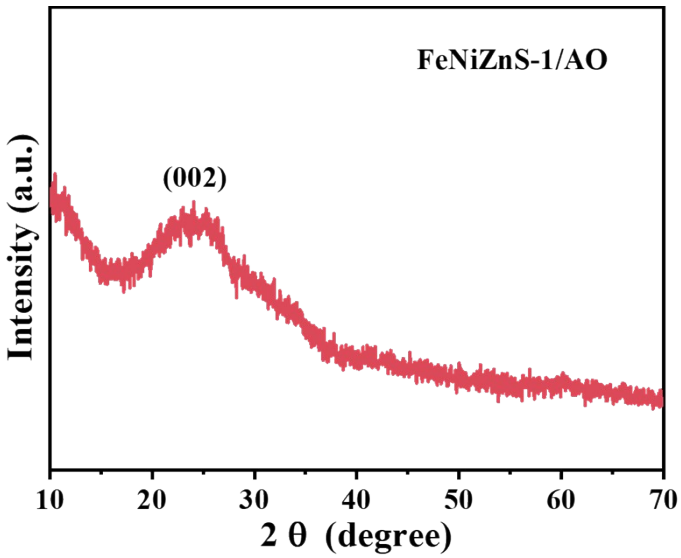

Figure. S16 XRD of pattern FeNiZnS-1/AO.

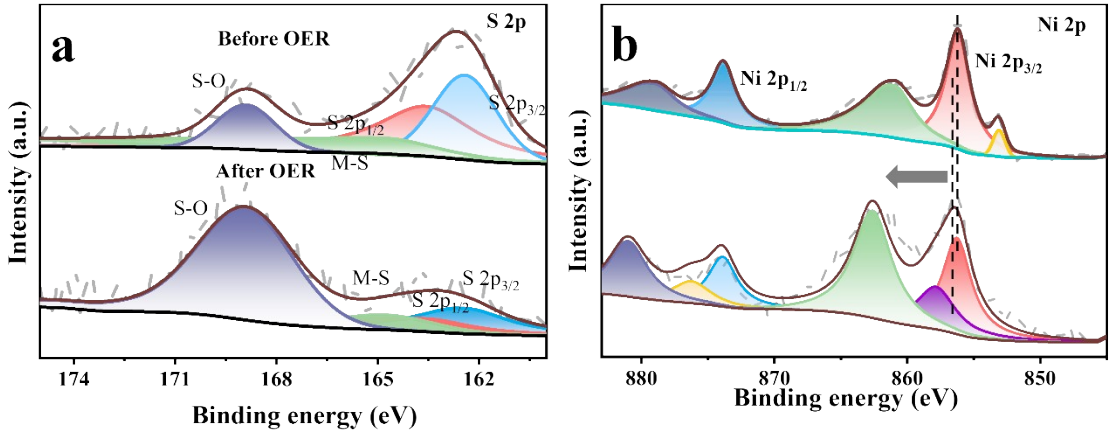

Figure. S17 XPS spectra of FeNiZnS-1/AO. (a) S 2p and (b) Ni 2p.

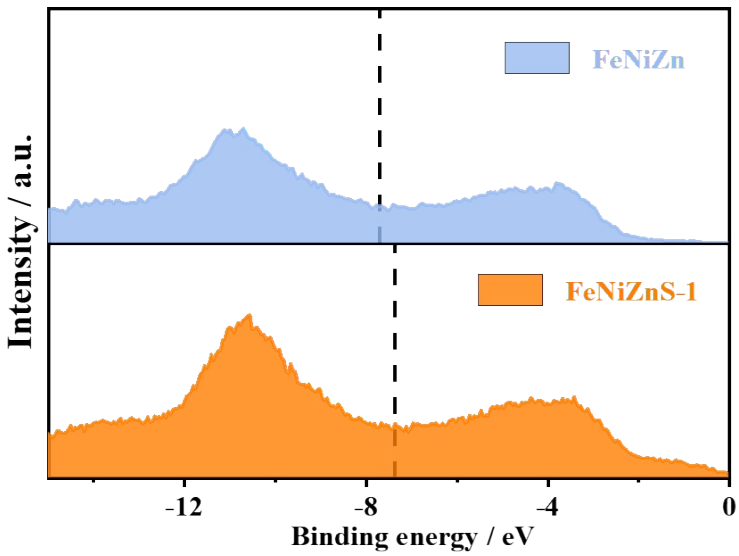

Figure. S18 The d-band centers are measured by HR-XPS.

References

1 F. Zheng, Z. Zhang, D. Xiang, P. Li, C. Du, Z. Zhuang, X. Li, W. Chen, Fe/Ni bimetal organic framework as efficient oxygen evolution catalyst with low overpotential, J Colloid Interface Sci 555 (2019) 541-547, https://doi.org10.1016/j.jcis.2019.08.005.

2 C.C. McCrory, S. Jung, I.M. Ferrer, S.M. Chatman, J.C. Peters, T.F. Jaramillo, Benchmarking hydrogen evolving reaction and oxygen evolving reaction electrocatalysts for solar water splitting devices, J Am Chem Soc 137(13) (2015) 4347-57, https://doi.org10.1021/ja510442p.

3 S.J. Hwang, S.-K. Kim, J.-G. Lee, S.-C. Lee, J.H. Jang, P. Kim, T.-H. Lim, Y.-E. Sung, S.J. Yoo, Role of electronic perturbation in stability and activity of Pt-based alloy nanocatalysts for oxygen reduction, J Am Chem Soc 134(48) (2012) 19508-19511, https://doi.org10.1021/ja307951y.

4 H. Xu, H. Shang, C. Wang, L. Jin, C. Chen, C. Wang, Y. Du, Three-dimensional open $CoMoO_x/CoMoS_x/CoS_x$ nanobox electrocatalysts for efficient oxygen evolution reaction, Appl. Catal. B 265 (2020), https://doi.org10.1016/j.apcatb.2020.118605.

5 R. Wang, J. Liu, J. Xie, Z. Cai, Y. Yu, Z. Zhang, X. Meng, C. Wang, X. Xu, J. Zou, Hollow nanocage with skeleton Ni-Fe sulfides modified by N-doped carbon quantum dots for enhancing mass transfer for oxygen electrocatalysis in zinc-air battery, Appl. Catal. B 324 (2023), https://doi.org10.1016/j.apcatb.2022.122230.

6 T. Bao, Y. Xia, J. Lu, C. Zhang, J. Wang, L. Yuan, Y. Zhang, C. Liu, C. Yu, A pacman-like titanium-doped cobalt sulfide hollow superstructure for electrocatalytic oxygen evolution, Small 18(4) (2021), https://doi.org10.1002/smll.202103106.

7 Y. Guo, X. Zhou, J. Tang, S. Tanaka, Y.V. Kaneti, J. Na, B. Jiang, Y. Yamauchi, Y. Bando, Y. Sugahara, Multiscale structural optimization: Highly efficient hollow iron-doped metal sulfide heterostructures as bifunctional electrocatalysts for water splitting, Nano Energy 75 (2020), https://doi.org10.1016/j.nanoen.2020.104913.

8 Y. Qian, J. Yu, F. Zhang, Z. Fei, H. Shi, D.J. Kang, H. Pang, Hierarchical binary metal sulfides nanoflakes decorated on graphene with precious-metal-like activity for water electrolysis, Chem. Eng. J 470 (2023), https://doi.org10.1016/j.cej.2023.144372.

9 K. Wan, J. Luo, W. Liu, T. Zhang, J. Arbiol, X. Zhang, P. Subramanian, Z. Fu, J. Fransaer, Metal-organic framework-derived cation regulation of metal sulfides for enhanced oxygen evolution activity, Chin J Catal 54 (2023) 290-297, https://doi.org10.1016/s1872-2067(23)64533-4.

10 Z. Wang, Y. Wang, N. Zhang, L. Ma, J. Sun, C. Yu, S. Liu, R. Jiang, Highly efficient oxygen evolution catalysis achieved by NiFe oxyhydroxide clusters anchored on carbon black, J. Mater. Chem. A 10(19) (2022) 10342-10349, https://doi.org10.1039/d2ta01931k.

11 F. Luo, Q. Zhang, X. Yu, S. Xiao, Y. Ling, H. Hu, L. Guo, Z. Yang, L. Huang, W. Cai, H. Cheng, Palladium phosphide as a stable and efficient electrocatalyst for overall water splitting, Angew. Chem. Int. Ed. 57(45) (2018) 14862-14867, https://doi.org10.1002/anie.201810102.

12 X. Li, X. Duan, C. Han, X. Fan, Y. Li, F. Zhang, G. Zhang, W. Peng, S. Wang, Chemical activation of nitrogen and sulfur Co-doped graphene as defect-rich carbocatalyst for electrochemical water splitting, Carbon 148 (2019) 540-549, https://doi.org10.1016/j.carbon.2019.04.021.

13 W.-D. Yang, R.-D. Zhao, F.-Y. Guo, J. Xiang, S. Loy, L. Liu, J.-Y. Dai, F.-F. Wu, Interface engineering of hybrid $ZnCo_2O_4$@$Ni_{2.5}Mo_6S_{6.7}$ structures for flexible energy storage and alkaline water splitting, Chem. Eng. J 454 (2023), https://doi.org10.1016/j.cej.2022.140458.